# A Discrete Multitone Transceiver System for HDSL Applications

Jacky S. Chow, *Student Member, IEEE*, Jerry C. Tu, *Student Member, IEEE*, and John M. Cioffi, *Senior Member, IEEE*

*Abstract*—**A discrete multitone (DMT) transceiver design for high-bit-rate digital subscriber line (HDSL) access is presented and analyzed. The DMT transmitter and receiver structure and algorithms are detailed, and the computational requirements of DMT for HDSL are estimated. We find that at a sampling rate of 640 kHz, using an appropriate combination of a short FIR equalizer and a length-512 DMT system, 1.6 Mb/s data transmission is possible within the CSA at an error rate of $10^{-7}$ on a single twisted pair. We also show significant performance margin can be achieved when two coordinated twisted pairs are used to deliver a total data rate of 1.6 Mb/s. We conclude that, in terms of a performance-per-computation figure of merit, the DMT system is an excellent candidate for HDSL implementation.**

## I. Introduction

MULTITONE modulation methods use an optimized frequency division allocation of energy and bits to maximize the reliably achievable data rates that can be transmitted over bandlimited communication channels. These systems are easily described because they use frequency division multiplexing to transport a single-input data stream on several carriers within the usable frequency band of the channel. The simplicity of multitone methods accounts for their use in some of the earliest data transmission modems, such as the Collin's Kineplex modems of 1957 [1]. While the simplicity and appeal of multitone modulation has existed for decades, it is only very recently that their optimal performance has been proven theoretically (see [2], [3]) and demonstrated in practice with recent products, such as Telebit's Trailblazer modems [4] or NEC's multitone voiceband and groupband modems [5]. These highest-performance products are sold at only a fraction of the cost of comparable performance single-channel or QAM modems.

The excellent high-performance/cost tradeoff of multitone modulation also makes it a strong candidate for the transceiver implementation for high-bit-rate digital subscriber lines (HDSL), a 1.6 Mb/s digital subscriber service on twisted-pair channels of up to two miles. This paper presents a multitone modulation structure that is of particularly high performance and low cost for the HDSL application. We generally find that, even on worst-case channels, a 1.6 Mb/s (1.536 Mb/s user data plus 64 kb/s control channel) data rate is achievable at an error rate of $10^{-7}$ on a single twisted pair (with 6 dB margin). Furthermore, we find that the described multitone system exhibits excellent margins (nearly 18 dB) for the so-called dual-duplex option of providing 1.6 Mb/s on two coordinated twisted pairs.[1]

The intersymbol interference, crosstalk, and attenuation of 24-gauge and/or 26-gauge twisted pair is particularly severe within the two-mile carrier serving area (CSA) requirements, as we discuss in Section II. Section II also briefly examines and reviews theoretically and practically achievable maximum data rates for HDSL. Equalization and coding methods have to be carefully applied in the HDSL application to render the high transported data rates reliable. In the approach presented, a particularly effective combination of a small amount of time-domain equalization and of a larger amount of multitone modulation is used to transmit the data reliably. The equalizer is used to shorten the effective response length of the data channel, while the multitone modulation is used to mitigate the remaining intersymbol interference and the effects of crosstalk, as is described in Section III. The multicarrier system is fully adaptive, employing both an adaptive algorithm for update of the adaptive filters and also a special channel identification procedure that is used to initialize and update the transmitter bit allocation to frequency-indexed subchannels. This relatively simple procedure is essential for maximizing performance. We also estimate the complexity in terms of the number of arithmetic operations in Section III and illustrate that the multitone transceiver can be implemented with programmable signal processors, although those processors may need to be custom designed for lowest cost.

The performance in achievable data rate of the multicarrier system is analyzed and characterized in Section IV as a function of input power, channel characteristic, number of tones or carriers, sampling rate, noise margins, and crosstalk.

Manuscript received November 14, 1990; revised May 17, 1991. This work was supported in part by a gift from Bell Communications and by a contract with the University Technology Transfer Institute.

The authors are with the Information Systems Laboratory, Department of Electrical Engineering, Stanford University, Stanford, CA 94305.

IEEE Log Number 9102134.

[1]We note that results in this paper use channel models with less attenuation than those of previous studies in [6]–[9], based on measured line results of several industrial sources.

0733-8716/91/0800-0895$01.00 © 1991 IEEE

## II. Subscriber Loop Characterization and Modeling

In any study of HDSL transceivers, the channel models are critical to specification of performance. We outline in detail the HDSL channel models used throughout the study of DMT HDSL transceivers. We note that performance projections based on different channel models can lead to erroneous claims and comparisons. A detailed tutorial on HDSL technologies is presented by Lechleider in this issue [10].

### A. CSA Loop Characteristics

The carrier serving area (CSA) is an identifiable subset of the current subscriber loop population in the U.S., and our HDSL study is restricted to loops that satisfy minimal CSA requirements. The CSA consists of mainly 24- and 26-gauge twisted pair, with lengths on 24-gauge wire to 12 kft and on 26-gauge wire to 9 kft. CSA loops can also contain bridge taps of limited length; a complete specification of the CSA appears in [11]. Impairments in the CSA data transmission channel include:

- intersymbol interference (ISI),
- crosstalk noise coupled from adjacent loops within the same cable bundle,
- impulsive noise (caused by switching transients, lightning, and other electrical machinery),
- echo noise resulting from the combination of imperfect hybrids and gauge changes on the line as well as signals reflected from bridged taps,
- electronics noise (such as quantization noise in analog-to-digital converters (ADC) and thermal noise in the analog portion of the transmitter and receiver), and
- inductive noise at 60 Hz and its harmonics caused by nearby power lines.

We consider a set of representative CSA channels, provided by Bell Communications Research [12], that have the respective loop cable arrangements illustrated in Fig. 1. We use a letter designation (*A–H*) on these channels for reference. These channels are generally representative of some of the worst, in terms of channel impulse response, expected to be found within the CSA limits. In general, longer wire length, smaller wire size, and presence of more and longer bridge taps results in poorer achievable data rates. We also note that on-premises wiring is often impossible to characterize statistically, so a 6 dB margin is imposed upon the performance of any HDSL transceiver to ensure that $10^{-7}$ error rate is maintained [13]. In all loop models in this paper, we include this 6 dB margin simply by increasing loop attenuation for the loops in Fig. 1 by 6 dB (see also Footnote 1).

### B. Channel Modeling

A line simulation program, based on standard transmission line modeling and a standard set of twisted-pair characteristics, was used to generate an impulse response for each of the channels in Fig. 1. The effect of the coupling transformer at each end of the loop termination was

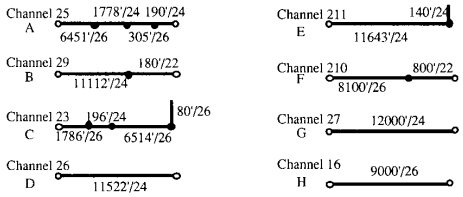


Fig. 1. CSA channels: length (in ft.)/gauge.

included by adding a double-pole double-zero highpass digital filter with a cutoff frequency of 300 Hz. These characteristics were found to be in near exact agreement with those provided by separate programs at various industrial groups working in the HDSL field [14], [12]. One such time-domain impulse response is shown in Fig. 2 for Channel *H*.

Crosstalk noise coupled from adjacent wire pairs in the cable bundle is the dominant noise impairment in CSA loops. Various characterizations have been proposed [15], [16], and we will use [15], which models crosstalk noise as near end crosstalk (NEXT) with the following transfer function:

$$|H_{\mathrm{NEXT}}(f)|^2 = K_{\mathrm{NEXT}} f^{3/2} \tag{1}$$

where $K_{\mathrm{NEXT}}$ is the coupling coefficient. Since far end crosstalk noise is attenuated by the channel, the resulting noise power is negligible compared to near end crosstalk. Hence, we will only consider NEXT. The coupling coefficient $K_{\mathrm{NEXT}}$ for a 50-pair cable was empirically determined to be approximately $10^{-13}$ [17].

To model the effects of residual echo after cancellation, we note that a typical CSA loop attenuation is on the order of 24 dB, and a good echo canceller can presumably reduce the echo to a level of 30–40 dB below the received signal. Assuming an average input power of 10 mW (10 dBm), this translates into $-44$ to $-54$ dBm of total echo noise power across the two-sided bandwidth of 640 kHz, which corresponds to a noise power spectral density of $6.22 \times 10^{-11}$ to $6.22 \times 10^{-12}$ mW/Hz. This residual echo noise is assumed to be additive white Gaussian noise (AWGN), and we fix this AWGN to have a power spectral density of $-110$ dBm/Hz for subsequent analysis and simulation. The electronics noise, as mentioned earlier, is typically on the order of $-140$ to $-170$ dBm/Hz [6] and is thus, by comparison to echo noise, negligible. Of course, crosstalk noise is larger than either echo or electronics noise.

While impulsive noise is more difficult to characterize, some [18] have attempted to model its effect. Impulsive noise usually consists of millivolt pulses (say, up to 40 mV) that last a few $\mu$s to 1000 $\mu$s.

Inductive noise can be modeled as a fixed noise level at 60 Hz, but the highpass filter simulating the transformers eliminates the inductive noise.

*1) Pole-Zero Modeling:* To facilitate simulation of CSA loops for performance analysis, we constructed a pole-zero (IIR) model for each channel impulse response

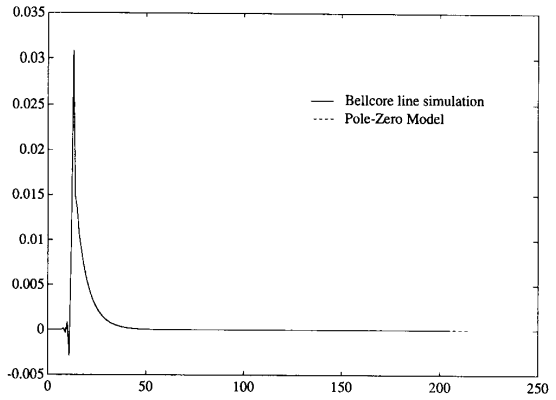


Fig. 2. Impulse response of a CSA loop.

at various sampling rates, using standard system identification tools. An impulse response obtained for Channel *H* is compared to the impulse response generated by a pole-zero model in Fig. 2. Since the pole-zero model closely approximates the true response, the use of pole-zero models for subsequent studies is justified.

The number of poles and zeroes varies with different CSA channels, but they all fall into the same range: 5–8 zeroes, and 6–12 poles. For future reference, assume the number of zeroes for a particular channel is equal to $\nu$, and the number of poles is equal to $L - 1$. We also found that most of the CSA channels are not minimum phase, i.e., some of the zeroes from the pole-zero models lie outside the unit circle in the $z$-plane.

### C. Capacity

The capacity of these loops with the aforementioned models is computed in [6], at the sampling rates of 400 and 800 kHz. As explained later in Section IV-A and [6], a sampling rate of 400 kHz is not sufficient to maximize the HDSL transceiver performance on most CSA channels shown in Fig. 1 as well as the capacity with a flat input spectrum (called "flat input capacity" in Table I) at 800 kHz sampling rate. The two columns under "Capacity" list the capacity using the optimal transmit power distribution [6], and represent the best data rates that can be achieved with an 800 kHz sampling rate. "Crosstalk Bound" assumes crosstalk noise is the only noise impairment (and, thus, ignores the contribution of AWGN), while "11 dBm Power" includes the effect of AWGN with 11 dBm transmit input power. The three columns under "Flat Input Capacity" do not optimize transmit power distribution; instead, a flat input power spectral density is assumed. The effects of near end crosstalk, 6 dB margin, and AWGN are included for the calculation, and the maximum achievable data rate based on the flat input power spectrum are shown for three different input powers: 1, 10, and 50 mW (0, 10, and 17 dBm, respectively). Notice that, with a sufficiently high input power (10 dBm or above), the penalty in achievable data rate

TABLE I
CAPACITY AND FLAT INPUT CAPACITY FOR CSA LOOPS, 800 KHZ RATE AND WITH 6 DB MARGIN (IN MB/S)

| | Capacity with 6 dB Margin | | Flat Input Capacity with 6 dB Margin | | |
|---|---|---|---|---|---|
| Channel | Crosstalk Bound | 11 dBm Power | 0 dBm Power | 10 dBm Power | 17 dBm Power |
| A | 2.42 | 2.30 | 1.87 | 2.29 | 2.40 |
| B | 2.39 | 2.27 | 1.85 | 2.27 | 2.37 |
| C | 2.32 | 2.20 | 1.78 | 2.19 | 2.30 |
| D | 2.31 | 2.19 | 1.77 | 2.19 | 2.29 |
| E | 2.26 | 2.14 | 1.72 | 2.13 | 2.24 |
| F | 2.29 | 2.17 | 1.75 | 2.16 | 2.27 |
| G | 2.19 | 2.07 | 1.65 | 2.06 | 2.16 |
| H | 2.14 | 2.02 | 1.60 | 2.01 | 2.11 |

(10 dBm or above), the penalty in achievable data rate without optimizing the transmit power distribution becomes negligible. Thus, we will assume a flat input power spectrum is used, and this will simplify analysis and simulation. Also, this allays any practical concern about loop-to-loop energy spectrum variation.

We can infer from this table that 1.6 Mb/s can be reliably transmitted over most CSA channels. However, an excellent transceiver design is required to accomplish this goal on either a single pair or on two coordinated pairs with a large performance margin such as 12 dB. Even with only a 6 dB performance margin on two pairs, 800 kb/s is 35–50% of capacity and more than a trivial receiver is required. On the other hand, a data rate of 160 kb/s on CSA channels (as in the case of basic rate ISDN) is well below the fundamental limits (although it may be a little more difficult on longer (18 kft) channels). Thus, one would not expect that a simple receiver used for basic rate ISDN would necessarily be good for use in HDSL.

## III. The Discrete Multitone Transceiver

This investigation focuses on a discrete multitone (DMT) transceiver for HDSL. We briefly describe the modulation and demodulation processes and the major system components. We also accurately compute computational requirements for the DMT HDSL transceiver using Motorola's 56000 DSP as a representative host for implementation. A system using multiple Motorola 56000 DSP's has been used to implement the described DMT transceiver in real-time at Stanford University.

### A. System Description

A simplified illustration of the DMT transmitter, receiver, and channel appears in Fig. 3. The basic concept is to use frequency division modulation to divide the transmission system into a set of frequency-indexed subchannels that appear to be modulated and demodulated independently. With a careful allocation of bits and transmit power to the subchannels, it is well known [2], [3] that such a system is capable of performing at the highest theoretical limits and that no other system can exceed its

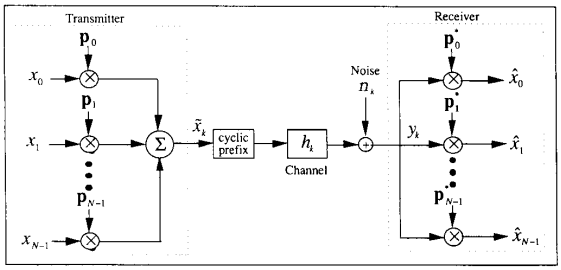


Fig. 3. Simplified illustration of DMT transceiver and channel.

performance. There are now at least three commercial 19.2 kb/s voiceband modems, marketed by three different companies, that use DMT to attain excellent performance. This section describes a DMT system for HDSL.

The system in Fig. 3 is presumed to be sampled (digitized) at a rate that is at least twice as high as any signal frequency, so that sampling theory arguments apply and the discrete-time system is equivalent to the actual continuous-time system. A *block* of input bits is divided into $N$ *subsymbols*, $x_n$, $n = 0, \cdots, N-1$, that are independently modulated by $N$-dimensional sampled-sinusoid *modulating vectors* $\boldsymbol{p}_n$, and then summed to form an $N$-dimensional block of modulated *transmit signal samples* $\tilde{x}_k$, $k = 0, \cdots, N-1$. The $n$th modulating vector is given by:

$$\boldsymbol{p}_n = [p_{n,0} \quad p_{n,1} \quad \cdots \quad p_{n,N-1}] \tag{2}$$

where

$$p_{n,k} \triangleq \frac{1}{\sqrt{N}} e^{+j(2\pi/N)kn} \qquad k, n = 0, \cdots, N-1 \tag{3}$$

the inverse discrete Fourier transform (IDFT) vector. To ensure a real-valued transmit signal, $\tilde{x}_k = \Re(\tilde{x}_k)$, it is necessary that we impose the constraint on the subsymbols that ($*$ denotes complex conjugate, $\Re$ denotes real part)

$$x_n = x_{N-n}^* \qquad n = 1, \cdots, N-1. \tag{4}$$

It is convenient to think of DMT as consisting of $N/2$ quadrature amplitude modulation (QAM) channels. In practice, of course, the modulation is done digitally and no explicit use of any carrier modulation frequencies or modulators is required. The *channel output samples* $y_k$ are found by the sum of the convolution of the modulated transmit samples, $\tilde{x}_k$, with the sampled channel *impulse response* $h_k$ and the additive noise $n_k$,

$$y_k = h_k * \tilde{x}_k + n_k. \tag{5}$$

The impulse response $h_k$ is assumed to be of finite length, and can be described by the $\nu + 1$ samples $h_0, \cdots, h_\nu$. Its *D-transform* is $h(D) = \Sigma_{k=0}^{\nu} h_k D^k$. In the receiver, the corresponding demodulation is accomplished by taking the inner product of the corresponding $N$ channel outputs, $y_0, \cdots, y_{N-1}$, with $\boldsymbol{p}_n^*$. The noise at the channel output presently includes only additive white Gaussian noise; we will generalize to the crosstalking case as this development proceeds.

Because of the finite number of subchannels, a *cyclic prefix* (CP) of the transmitted signal samples $\tilde{x}_k$ is needed once for every transmitted block of bits. The CP prefixes the block of transmitted samples $\tilde{x}_0, \cdots, \tilde{x}_{N-1}$ by the (repeated) samples, $\tilde{x}_{N-\nu}, \cdots, \tilde{x}_{N-1}$. We denote the corresponding time indexes at the beginning of the block by $k = -\nu, -\nu+1, \cdots, -1$. When $\nu + 1$ is the length of the channel impulse response in sample periods, then the successive blocks of transmitted data do not interfere with each other, and one can write (see [3]) that

$$\hat{x}_n = |H_n| x_n + n_n \tag{6}$$

where

$$H_n = h_0 + h_1 e^{-j(2\pi/N)n} + h_2 e^{-j(2\pi/N)n} + \cdots + h_\nu e^{-j(2\pi/N)\nu n}. \tag{7}$$

In practice, the modulation and demodulation processing is implemented with fast Fourier transform (FFT) algorithms that require significantly less computations than would occur in the direct implementation shown in Fig. 3. We discuss specific computational requirements in Section III-C.

A trellis code [19] of coding gain $\gamma$ can be applied to each subchannel so that the energy allocated to this channel will sustain a greater number of bits than in the absence of the applied trellis code. The number of bits can be approximated by

$$b_n = \log_2\left(1 + \frac{\mathrm{SNR}_n}{\Gamma}\right) \tag{8}$$

where $\Gamma = 10\ \mathrm{dB} - \gamma$ for a bit error rate of $10^{-7}$ [20]. If no code is used, $\gamma = 0$ dB and $\Gamma = 10$ dB. The *signal-to-noise ratio* on the $n$th subchannel is denoted by $\mathrm{SNR}_n$ and is computed by

$$\mathrm{SNR}_n = \frac{\epsilon_x |H_n|^2}{\sigma^2} \tag{9}$$

where $\epsilon_x = E|x_n|^2$ is the signal energy of the $n$th subsymbol and $\sigma^2$ is the corresponding white noise energy. In practice with HDSL, the dominant noise is crosstalk noise, which is not white, so that $\sigma^2 \to \sigma_n^2$, a subchannel-dependent noise energy. When $N$ is chosen sufficiently large, the noise on each of the subchannels will be approximately white within the occupied frequency band and will be uncorrelated with the noise on any of the other subchannels. In order to compute the bit allocation outlined by (8), the channel characteristic must be known at the transmitter, which is achieved as described in Section III-A-3. The energy allocation is approximated by a flat

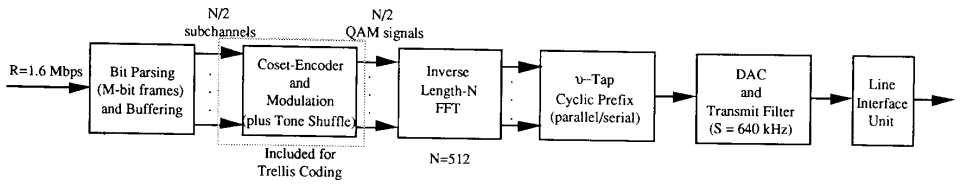


Fig. 4. Block diagram of a specific DMT HDSL transmitter.

transmit energy spectrum, so that $\epsilon_x$ is not a function of the frequency index $n$. Our studies have found that very little is lost in using this flat energy distribution in the HDSL application. The poorest subchannels carry only dummy data and are simply ignored by the receiver. This flat transmit spectrum has the effect of rendering the crosstalk power spectrum from any DMT HDSL transmitter constant in practice.

*1) The DMT HDSL Transmitter:* A specific embodiment of the HDSL transmitter is illustrated in block diagram form in Fig. 4. In the specific implementation of the system that we study, $\nu$ is always limited (through equalization, as discussed later) to a maximum of 8, and later in Section IV-A-3) and 4), we fix the sampling rate $S$ to be equal to 640 kHz and $N = 512$.

For a single twisted pair to carry $R = 1.6$ Mb/s (the *single-duplex* option), the input data bit stream is parsed into $M$-bit blocks, where $M = (N + \nu)R/S = 1300$. These bits are then transformed into (a maximum of) $N/2 = 256$ QAM subsymbols that are then applied to a trellis encoder. The trellis coder sequentially processes the frequency-indexed subsymbols to avoid the large latency and memory requirement that would occur with multiple trellis encoders. This process requires that the subchannel indexes be "shuffled" to avoid any minor correlation between the noise on adjacent frequency subchannels. The output of the trellis encoder is then modulated, as described earlier, through the use of an $N = 512$ inverse FFT. Finally, an eight-sample cyclic prefix is placed in the beginning of the corresponding block of modulated transmit samples, and the extended block of $N + \nu$ samples is then applied to the channel through the digital-to-analog converter (DAC) and line-interface unit. The sampling rate is 640 kHz, which leaves the 256 subchannels effectively separated by 1.25 kHz. This corresponds to a *block symbol period* of $512 + 8 = 520$ samples or 812.5 $\mu$s. Eight samples is considerably shorter than most HDSL channel impulse responses at 640 kHz. An unusual and simple equalizer is used in the receiver to contain intersymbol interference to eight samples, or impulse-response length to nine samples.

For the so-called *dual-duplex* option with two twisted pairs, the 1300-bit blocks are parsed into the 512 QAM subchannels that exist on both of the channels. There are then two IFFT's, two DAC's, and two line-interface units. However, only one trellis code is necessary with this option with respect to the single-duplex option. This improves the performance margin but increases the cost of the dual-duplex option. If a sufficient margin can be obtained using the single-pair solution (called "single-duplex"), then it is preferable from a cost standpoint.

*2) The DMT HDSL Receiver:* A block diagram of the general DMT HDSL receiver appears in Fig. 5, and a specific receiver that corresponds to the specific transmitter of Fig. 4 is shown in Fig. 6. This receiver structure is a slight variation of the original receiver proposed in [7]. Both receiver structures achieve the same performance but the one in Fig. 6 results in lower complexity.

An actual HDSL channel response is of significant duration in practice, and we can model its polynomial-fraction $D$-transform

$$\tilde{h}(D) = \frac{a(D)}{p(D)}. \tag{10}$$

In practice, we identify this infinite-impulse-response model, $\tilde{h}(D)$, by choosing $a(D)$ and $p(D)$ to minimize the mean square error between this model and the channel output. Using this method, the crosstalk noise also affects the settings for $a(D)$ and $p(D)$. Due to the nonminimum phase nature of $a(D)$, the use of an IIR equalizer $1/\tilde{h}(D)$ to eliminate ISI results in unstable filter. A short, fixed $L$-tap feedforward equalizer is thus used to process the sampled channel output $y_k$ sequentially. This equalizer does not remove intersymbol interference completely, but rather confines the impulse response so that its length is approximately $\nu + 1$ sample periods or less. By setting the equalizer to $p(D)$, we will have a minimum mean square error approximation of an additive white noise channel with impulse response characterized by $a(D)$, which has a response length of $\nu + 1$ sample periods or less. The last $N$ samples of the $N + \nu$ samples that correspond to the transmit block are extracted from the equalizer output. An $N$-point FFT is performed on the equalizer output. The FFT outputs, $z_n$, $(n = 0, 1, \cdots, N - 1)$, are multiplied by $N$ complex, 1-tap adaptive filters, $w_n$, $(n = 0, 1, \cdots, N - 1)$ so that a common decision device can be used to estimate the subsymbols on each of the subchannels. The initial tap setting for $w_n$

subchannels, then two IFFT's, two DAC's

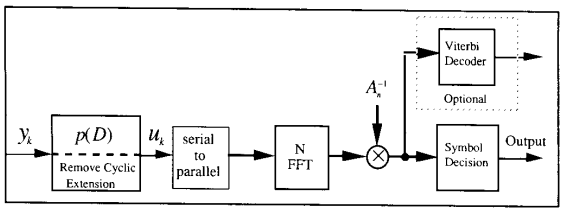


Fig. 5. Block diagram of the receiver.

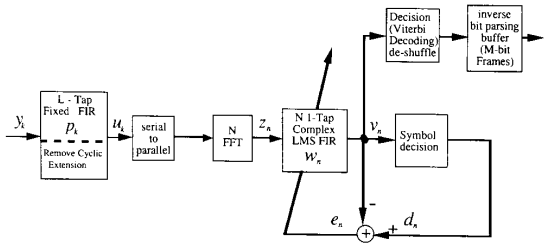


Fig. 6. Specific block diagram of a DMT HDSL receiver.

is:

$$w_n = A_n^{-1}, \qquad n = 0, 1, \cdots, N-1 \tag{11}$$

where

$$A_n = \sum_{k=0}^{N-1} a_k e^{-j(2\pi/N)kn}, \qquad n = 0, 1, \cdots, N-1 \tag{12}$$

the FFT of $a(D)$. The resulting output data

$$v_n = w_n z_n, \qquad n = 0, 1, \cdots, N-1 \tag{13}$$

can then be decoded, which in the case of an applied trellis code requires a Viterbi decoder as shown. The symbol decisions are used (in the coded case) only to derive an error signal, so that the adaptive updating mechanism can be used to allow for slight channel variation. The corresponding error is

$$e_n = d_n - v_n, \qquad n = 0, 1, \cdots, N-1. \tag{14}$$

Standard LMS algorithm can be used for updating,

$$w_n \leftarrow w_n + 2\mu_n e_n z_n^*, \qquad n = 0, 1, \cdots, N-1 \tag{15}$$

where $\mu_n$ is the stepsize for each subchannel, and can be adjusted independently to optimize the rate of convergence.

Since $a_k$ and $u_k$ are real, $A_n = A_{N-n}^*$ and $z_n = z_{N-n}^*$, so that (13)–(15) are computed only through $n = N/2$.

*3) Channel Identification and Initialization Protocol:* As the DMT transmitter requires knowledge (either directly, or indirectly through knowing the bit allocation $b_n$) of the channel, the channel impulse response and crosstalk noise spectrum must be estimated during initialization. The more accurate the initial estimate, the more reliable the transmission with DMT. Accuracy requirements are significantly mitigated by the adaptive filters in the receiver in practice, but are still important. (We note that decision feedback approaches that employ Tomlinson precoding [21], [22] also need to know the channel at the transmit side and require an even greater accuracy than DMT [8], even when an adaptive feedforward section is used in the DFE receiver.) Rather than pursue channel identification in detail (see, for example, [23]–[25] for details), we will briefly summarize the basic steps in the initialization protocol. The complete startup time (including channel identification, SNR calculation, and bit and energy allocation) is less than one second.

1) After receiving a request for transmission signal, some loopback and test patterns are exchanged, followed by timing and synchronization patterns.

2) A predefined pseudorandom sequence is sent from the transmitter to the receiver for spectral estimation. A pole-zero model for the channel is derived from the received training pattern using a least-squares fit.

3) Based on the result of the above channel spectral estimation, the receiver sets the tap values for the equalizer at the pole settings of the pole-zero model, then computes the SNR for each frequency-indexed subchannel, and finally computes the transmit bit and energy allocation across the frequency band.

4) The bit assignments are sent to the transmitter in a reliable fashion.

5) For bidirectional transmission, the above steps are repeated for the other direction.

6) After frame synchronization and start commands are exchanged, the DMT transceiver system is ready for actual data transmission.

We have not considered the implementation of echo cancellation in this paper. We note that low-computation/high-performance echo cancellation is possible with DMT (see [26]).

### B. Transmit Power Level

As shown in Section IV-A, we can improve performance by increasing the average input power. However, due to physical constraints, only a certain range of average input power level is feasible. As a result, maximum average input power or energy is a common constraint that is usually imposed at the input of the channel (or equivalently, at the output of the transmitter).

*1) Transmit Power Adjustment:* We have assumed an average energy constraint of $E_x$ per transmitted subsymbol, before adding the cyclic prefix. The IFFT and FFT do not change the energy of a block of data, so the energy constraint specified at the output of the IFFT in the transmitter is the same as at the input of the IFFT, i.e., the total average energy per block at the input of the IFFT is limited to $N\epsilon_x$. However, the total average energy of a $\nu$-sample cyclic prefix is not necessarily equal to $\nu\epsilon_x$. We will thus briefly investigate the impact of the cyclic extension samples to the average energy constraint.

The real and imaginary parts of the noise variance after the FFT in the receiver are, in general, unequal for any

specific frequency band due to the correlated, non-i.i.d. crosstalk noise at the input to the FFT. This inequality of variance is more profound at smaller blocklength (larger than 4), and the difference between the real and imaginary noise variance gradually diminishes as longer blocklength is used. As blocklength approaches infinity, the difference becomes zero. To optimize bit error rate throughout the subchannels, we would then need to assign unequal signal energy on the real and imaginary part of each frequency band. A fairly tight bound for the average energy of a block of $N + \nu$ samples (after cyclic extension) is derived in the Appendix.

However, as the blocklength increases, the difference between the real and imaginary noise variance becomes insignificant, and we can simply assign equal energy on the real and imaginary parts of each corresponding frequency band without any noticeable performance degradation. In this case, as derived in the Appendix, each sample at the output of the IFFT has the same average energy $\epsilon_x$. Consequently, the $\nu$-sample cyclic prefix does not change the energy constraint.

### C. Computation Requirements

In this section, we describe the computational requirements to implement the DMT transceiver. The computational complexity includes only the functions that are unique to DMT; those functions that are common to both DMT and conventional single-carrier transceivers are not included.

The following are the assumptions in computing the total complexity.

- Complexity is measured in terms of millions of instructions per second (MIPS).
- The sampling rate is equal to 640 kHz. We choose this number because, as Section IV-A shows, further increase in sampling rate does not significantly increase the throughput but does increase the cost substantially.
- A real addition, a real multiplication, or a real multiplication followed by a real addition (multiply–accumulate) is counted as one instruction; a complex multiplication is counted as four instructions.
- The number of required instructions to compute an $N$-point real-input FFT (or, equivalently, $N$-point real output IFFT) is assumed to be $N \log_2 N$, where $N$ is less than or equal to 128. Otherwise, the number of instructions is equal to $1.5N \log_2 N$ ($N$ is a power of 2).
- Computations required in synchronization, timing recovery, decision block, and coding/decoding are not included, since these components are common to other schemes such as DFE and thus have no impact on our comparison study.
- The echo canceller, which is required for single-duplex and dual-duplex options, is discussed separately in [26] and has a comparable complexity to the echo canceller used in baseband systems. We note that the complexity of echo cancellation can be significantly reduced in either case using the methods of [27] or [28].

TABLE II
IFFT TRANSMITTER COMPLEXITY AT 640 KHZ SAMPLING RATE

| IFFT Size ($N$) | 64 | 128 | 256 | 512 | 1024 |
|---|---|---|---|---|---|
| Complexity (in MIPS) | 3.8 | 4.5 | 7.7 | 8.6 | 9.6 |

TABLE III
RECEIVER COMPLEXITY AT 640 KHZ

| Complexity (in MIPS) | $L = 5$ | $L = 10$ | $L = 16$ | $L = 32$ | $L = 64$ |
|---|---|---|---|---|---|
| $N = 64$ | 9.67 | 12.5 | 15.9 | 25.0 | 43.2 |
| $N = 128$ | 10.8 | 13.9 | 17.5 | 27.1 | 46.4 |
| $N = 256$ | 14.3 | 17.4 | 21.1 | 31.0 | 50.9 |
| $N = 512$ | 15.4 | 18.6 | 22.4 | 32.5 | 52.6 |
| $N = 1024$ | 16.5 | 19.7 | 23.5 | 33.7 | 54.0 |

Thus, we focus on only the major transmit and receive functions that are significantly different from other schemes in estimating the computational requirement. Computations for pole-zero channel estimation, SNR calculation, and bit and energy allocation during the startup protocol are not included, as they are done "off-line" and have no effect during actual data transmission. We note that an FFT peripheral for the DSP would be of great significance in further lowering the listed computational requirements to follow.

*1) Transmitter Complexity:* The major transmit function is the IFFT that is performed once per block. The computational requirement of the transmitter is summarized in Table II.

*2) Receiver Complexity:* For a block of $N + \nu$ received data, $NL$ instructions are required for computing the outputs $u_0, \cdots, u_{N-1}$, and $1.5N \log_2 N$ instructions are needed for the $N$-point real input FFT. Recall that (13)–(15) are computed only through $n = N/2$, and so only $2N$ instructions are required to compute $v_n$, (13), $N$ instructions for obtaining the error samples, and $3N$ instructions for updating the weights. The complexity of the receiver is shown in Table III with these stated assumptions.

As mentioned earlier, a fairly accurate channel response can be modeled with about $\nu = 8$ zeroes and $L = 10$ poles, and a blocklength on the order of $N = 512$ would be sufficient; so the total computational power under the stated assumptions for the receiver is about 20 MIPS, which is fairly modest by today's standards.

## IV. PERFORMANCE AND DISCUSSION

In this section, we will analyze the performance of the DMT transceiver system. Various parameters that affect the performance are examined: coding, average input power, blocklength,[2] sampling rate, noise margins, and HDSL occupancy. We then focus on the tradeoff between performance and cost. Other techniques that could achieve similar performance are compared.

[2]Throughout this paper, blocklength refers to the size of the data block after adding the cyclic prefix, i.e., blocklength = $N + \nu$.

subch... then two IFFT's, two ...

### A. Performance Evaluation

In our analysis, we include ISI, AWGN, and near end crosstalk noise as impairments for the channels. We also separately consider impulsive noise. As described in Section II-B, the near end crosstalk has the transfer function $10^{-13}f^{3/2}$, and the AWGN is assumed to be at $-110$ dBm/Hz. We also note that the maximum achievable data rate is very close to capacity when using a flat transmit power spectrum as long as adequate input power is used, on all the CSA loops of interest (see Table I). Thus, we use a flat power spectrum at the channel input, over the utilized transmit bandwidth. We assume a mix of 25% HDSL service, 25% basic access, and 50% voice-grade service in a typical cable bundle. When 25% HDSL occupancy is exceeded, telephone company managers will elect to replace the bundle with fiber. The crosstalk noise power spectral density, $PSD_{\text{NEXT}}$, based on the assumption that all users who subscribe the HDSL service utilize the same signaling strategy and transmit power, is then equal to

$$PSD_{\text{NEXT}} = \begin{cases} PSD_{\text{in}}\, 10^{-13}f^{3/2}, & f \le 50 \text{ kHz} \\ \dfrac{PSD_{\text{in}}}{4}\, 10^{-13}f^{3/2}, & f > 50 \text{ kHz} \end{cases} \tag{16}$$

where $PSD_{\text{in}}$ is the input signal power spectral density, and a 50 kHz cutoff frequency is assumed for services other than HDSL. For the DMT system, this occupancy assumption is also justified by the fact that a length 512 DMT system has considerably enhanced immunity to impulsive noise than symbol-by-symbol modulation approaches, as discussed later in this section. Thus, an artificially high crosstalk margin or gain is redundant in the DMT system, so we use only 6 dB to cover the case of unknown on-premises wiring. Signal, crosstalk noise, and AWGN are processed by the equalizer, which has a fixed taps setting equal to the least-squares pole polynomial of the channel. After the signal-to-noise ratio (SNR) for each QAM subchannel is obtained, we calculate the number of levels assigned to each QAM subsystem by the following equation [29], [8]:

Number of levels for subchannel

$$j \triangleq L_j = \frac{3\ \text{SNR}_j}{[Q^{-1}(\text{BER})]^2} + 1 \tag{17}$$

where BER is the desired error rate, which we set to $10^{-7}$, and

$$Q(a) \triangleq \int_a^{\infty} \frac{1}{\sqrt{2\pi}} e^{-x^2/2}\, dx. \tag{18}$$

Equation (17) is valid as long as the noise is additive Gaussian noise [30]. We also implicitly assume the number of the nearest neighbor is equal to 1, and coding gains of any applied codes with higher nearest neighbor counts can be correspondingly reduced by an appropriate factor. The number of bits, $b_j$, assigned to subchannel $j$ is then

$$b_j = \log_2 L_j. \tag{19}$$

In general, $b_j$ is not an integer; we can either truncate it to an integer, or (in the coded case) we can round it to the nearest fraction (such as 3.25 bits per $2D$ symbol) that can be implemented by multidimensional trellis codes [31], [8]. The total data rate, $R$, (in bits/second) is obtained:

$$R = \frac{S}{N + \nu} \sum_j b_j \tag{20}$$

where $S$ is the sampling rate.

The performance of a representative set of CSA loops, as shown in Fig. 1, is evaluated analytically with different system parameters. Without coding and with a sampling rate of 640 kHz, the achievable data rates as a function of average input power are shown in Fig. 7. Use of small gauge (26g) wire and the existence of bridge taps severely limit the data rates of this set of "lossy" end of the local loops. Channel $H$, which consists of 9000 feet of 26-gauge wire, has the poorest performance among the set of channels, and we will focus on this channel for the remainder of this section, since the performance results of Channel $H$ can serve as a "lower bound" for the other channels considered.

*1) Coding:* As shown in Fig. 7, only some of the channels studied achieve the objective 1.6 Mb/s data rate with 6 dB margin without a code, using one twisted pair. With two twisted pairs, however, the T1 rate can be achieved without code. Since the achievable data rate is approximately doubled when using two twisted pairs instead of a single wire-pair, we will from here on focus on the single twisted-pair case. However, when considering the dual-duplex twisted pair case, one only needs to look at performance in our plots at 800 kb/s instead of 1.6 Mb/s. A trellis code can be used to improve the data rate. We consider two codes: a four-dimensional sixteen-state 4.5 dB gain trellis code and a more powerful four-dimensional 5.5 dB gain trellis code, which presumes use of some good shaping code, as described in [32]. We assume the loss due to the increase of the number of nearest neighbors is offset by shaping gains [19], so that an effective gain of 4.5 and 5.5 dB, respectively, are assumed for the two codes. At lower bits per subchannel, the four-dimensional code has a higher minimum distance when there are no parallel transitions in the trellis describing the code. Thus, while it is readily possible to achieve shaping gain at lower bits per subchannel, the coding gain of the original code is higher and compensates for the lack of shaping gain in the common four-dimensional code. The effect of concatenating a trellis code to the DMT system on Channel $H$ is shown in Fig. 8 using a blocklength of 520 and a sampling rate of 640 kHz. With the powerful 5.5 dB trellis code, this 9000 ft 26-gauge channel can achieve the T1 rate with significant margin.

As described earlier, different number of bits are assigned to the subchannels according to the SNR of each

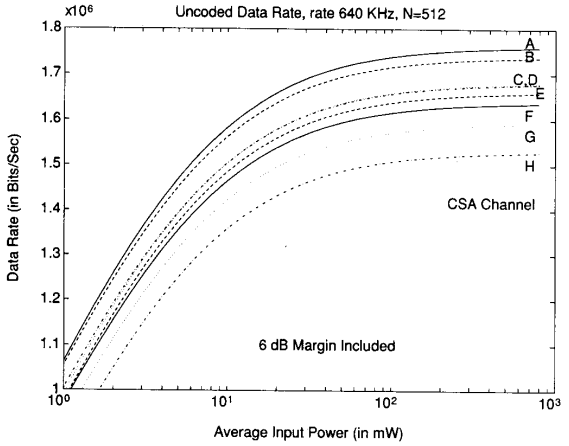


Fig. 7. Uncoded data rate for CSA channels (6 dB margin included).

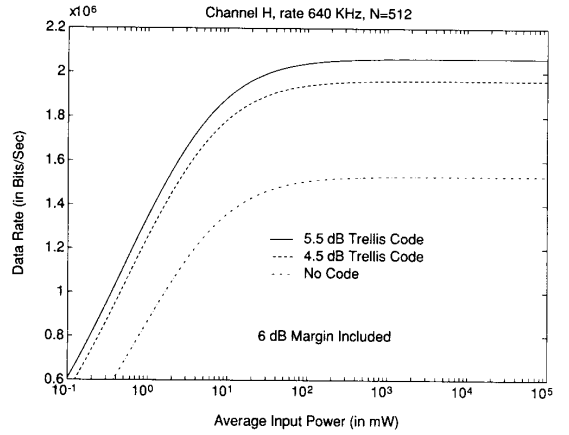


Fig. 8. Effect of coding and average input power on data rate (6 dB margin included).

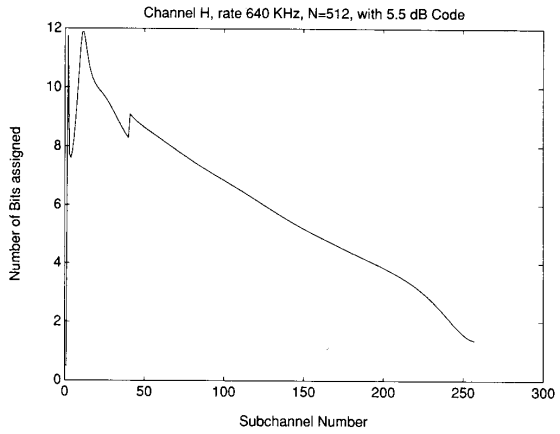


Fig. 9. Bit distribution of channel $H$ with 5.5 dB code.

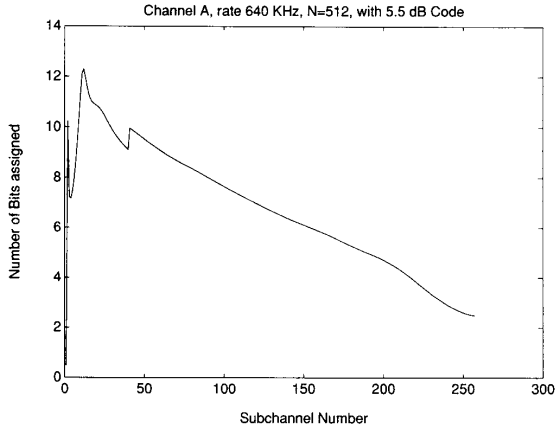


Fig. 10. Bit distribution of channel $A$ with 5.5 dB code.

subchannel. However, the number of bits assigned to any subchannel cannot be arbitrarily large, as an unrealisticlly large signal point constellation would have to be used. We therefore propose that a maximum of 10 information bits should be used in any subchannel. Fig. 9 shows the information bit distribution of Channel $H$, with a 5.5 dB code. The achievable data rate decreases by less than 1% when we apply the limit of 10 information bits/subchannel. Even for the best channel (Channel $A$; see Fig. 10), the loss in throughput is only slightly above 1%. We thus conclude that the bit assignment can be implemented practically.

*2) Average Input Power:* The achievable data rate of Channel $H$ is plotted against average input power in Fig. 8. We observe that, while the data rate generally improves with increasing input power, the improvement is significant in the very low input power region and becomes minimal at very high input power. The reason is that we assume all users of the CSA loops within the same 50-wire bundle utilize the same signaling strategy and transmitter power [assuming the same earlier HDSL occupancy in (16)]. As a result, the crosstalk noise that results from interfering neighbors that employ the same scheme is directly proportional to the input power used. With very low input power, the resulting crosstalk noise is so small that the dominating impairment becomes the AWGN, and within this region an increase of input power directly improves the SNR and thus the data rate improves noticeably. However, as input power increases further, the crosstalk noise becomes comparable and finally dominates the AWGN, and over this crosstalk-dominating region, increase in input power causes a corresponding increase in the crosstalk noise. As a result, there is virtually no net gain in achievable data rate in the very high input power region. An average power in the range of 10–50 mW is sufficient to transmit high data rates reliably, and physical limitations favor the use of lower input power. We thus decide on using 10 mW as the average input power.

then two IFFT's, two

*3) Blocklength:* We expect a higher data rate as longer blocklength is used, as shown in Fig. 11 for Channel $H$ with 10 mW of input power and a 640 kHz sampling rate. However, the higher complexity, increased memory requirements, and inherently longer delay required for long blocklengths make it unattractive for practical systems. We conclude that a blocklength of 520 (512 plus cyclic extension) is sufficient to provide enough frequency resolution, while simultaneously maintaining reasonable cost and delay. We note that even blocklengths as low as 128 and 256 (plus cyclic prefix) will also achieve near-optimal performance.

*4) Sampling Rate:* Sampling rate has a profound impact on the maximum achievable data rate. A low sampling rate forces a large number of bits to be squeezed into a limited bandwidth, and this can significantly lower the performance.

As an example, the total number of bits per block (assuming use of the same blocklength) has to double in order to maintain the same data rate if we halve the sampling rate, but to double the total number of bits would require an exponential increase in signal-to-noise ratio (SNR) in order to keep the same bit error rate. Although the crosstalk noise is less with a lower sampling rate because of the $f^{3/2}$ frequency dependency, the improvement in SNR is not sufficient to secure the bit error rates. Since we fix BER $= 10^{-7}$ as a criterion, this implies that we will not be able to keep the data rate as desired.

This phenomenon is clearly depicted in Fig. 12, where the throughput of Channel $H$ is plotted against different sampling rates with a 5.5 dB trellis code. This figure is generated with a set of pole-zero models derived for Channel $H$ at the following sampling rates: 200, 250, 400, 512, 600, 640, and 800 kHz. We observe that by going from 400 kHz down to 200 kHz, for example, the data rate decreases by more than 30%, a clear indication that the sampling rate was too low. On the other hand, as the sampling rate increases, crosstalk noise becomes more severe at the higher frequency indexes and eventually degrades the SNR to a point that it may no longer be practical to assign any bits to those frequency subchannels. The improvements, in terms of achievable data rate as we increase the sampling rate further, become negligible since the added bandwidth contributes little to the system while the cost of implementing the system keeps on increasing. As a reasonable compromise between performance and cost, we choose 640 kHz as the sampling rate for the DMT system. We note that DMT is not sensitive (at practical transmit power for HDSL) to picking the sampling rate too high, and that 640 kHz is sufficiently high. On the other hand, decision feedback approaches (in particular, those based on baseband PAM (2B1Q) [21] or carrierless QAM [22]) are sensitive to optimum choice of the sampling rate (see [20]) and that sampling too high or too low is not optimum with these approaches. In practice, voiceband modems that use decision feedback equalizers do vary the sampling rate. However, variation of sampling rate in HDSL is impractical, yielding a significant advantage of DMT with respect to decision feedback approaches.

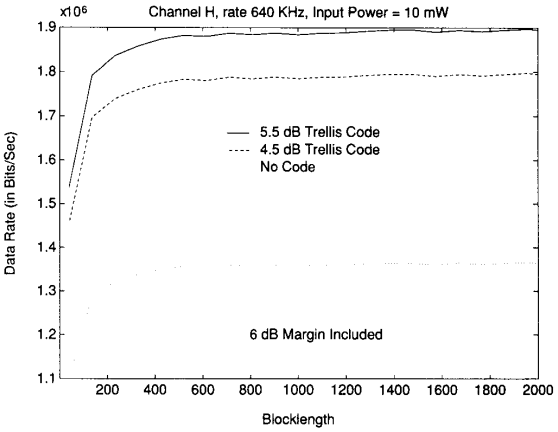


Fig. 11. Effect of different blocklength on data rate (6 dB margin included).

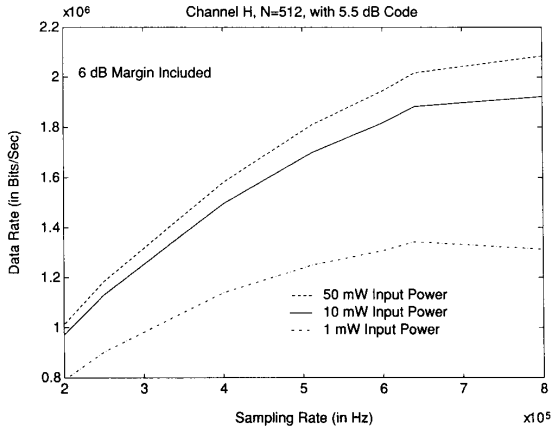


Fig. 12. Effect of sampling rate on data rate (6 dB margin included).

*5) Noise Margins:* As mentioned in Section II-B, we do not attempt to model all possible impairments that may be presented in the system: impairments such as nonlinearity and impulsive noise are not included (so far). In addition, the models that are included for the impairments may not always predict the noise accurately. As Bellcore suggested [11], some kind of margin is desirable in order to ensure that the actual performance will not degrade below an acceptable level. We have thus included a 6 dB margin throughout Section IV-A. In this section, we examine the noise margin further by increasing the crosstalk coupling coefficient $K_{\text{NEXT}}$ by a factor of 2 for an additional 3 dB noise margin, a factor of 4 for an additional 6 dB noise margin, and a factor of 16 for an additional 12 dB noise margin. The achievable data rate based on these new crosstalk coupling coefficients are calculated and Fig. 13 shows the results for Channel $H$ with a 5.5 dB code. The throughput drops to about 1.4 Mb/s with a 12 dB

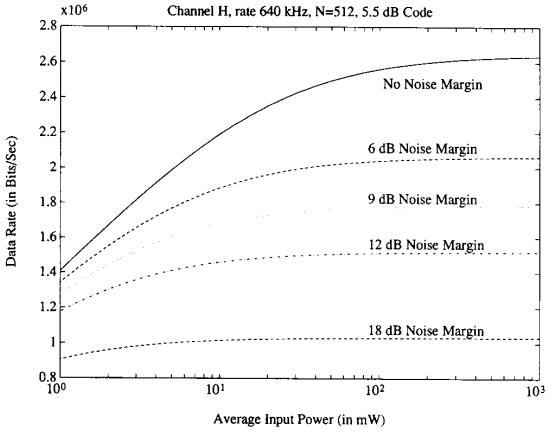


Fig. 13. Effect of noise margins on data rate.

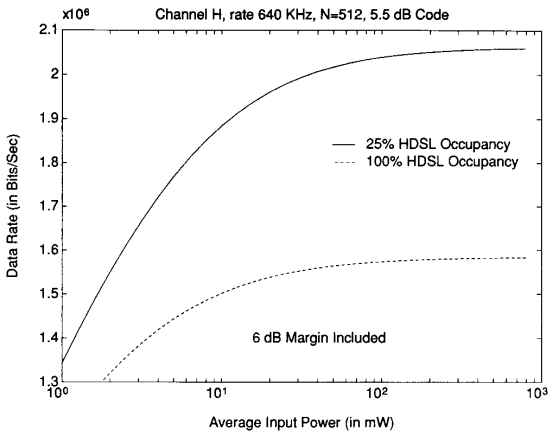


Fig. 14. Effect of HDSL occupancy on data rate (6 dB margin included).

margin and down to about 1 Mb/s with a 18 dB margin, but it is still possible to achieve 1.6 Mb/s with a 9 dB margin. Other CSA channels show similar performance degradation but at higher data rates. Overall, 99% of the CSA loops have a theoretical margin of approximately 9 dB for a single wire-pair, and over 18 dB margin with two coordinated twisted pair (dual-duplex).

*6) HDSL Occupancy:* Throughout the analysis, we have assumed the cable bundle is 25% HDSL occupancy, a realistic assumption for the next 10 years ahead. We now investigate the worst-case scenario: 100% HDSL occupancy, where the near end crosstalk is most severe. We model this effect by modifying (16) to

$$PSD_{\text{NEXT}} = PSD_{\text{in}}\, 10^{-13} f^{3/2}. \tag{21}$$

The resulting throughput is shown in Fig. 14 for Channel *H*. The achievable data rate drops down to about 1.5 Mb/s with a 6 dB noise margin. This situation is not expected to occur in practice, as a bundle with high HDSL occupancy will be replaced by fiber for telephone company cost reasons.

*7) Impulsive Noise:* Discrete multitone modulation has an inherent tolerance to impulse noise, especially when the duration of the impulse is less than one block length in sample periods. The immunity to a very short burst (only one sample affected) is easily computed to be

$$\text{Impulse Margin} = 10 * \log_{10}(N)\ \text{dB} \tag{22}$$

with respect to one-dimensional modulation (like 2B1Q). The margin is $10 * \log_{10}(N/2)$ with respect to any QAM approach. This means that the variance of the impulsive noise sample must exceed the crosstalk noise level nominally present by an amount that makes the total noise sample variance $10 \log_{10}(N)$ larger. For $N = 512$, these margins are 27 and 24 dB, respectively, far in excess of the 12 dB normally quoted. In practice, impulsive noise can span many sampling periods, especially at the high sampling rates used in HDSL. A long impulse might span as many as 40 sampling periods at 640 kHz. Some particularly bad impulses could exceed one blocklength. For an impulse of 40 samples, the above margins would reduce to approximately 13 and 10 dB, respectively. Nevertheless, these numbers are still excellent with respect to decision feedback approaches. To the extent that margins quoted for HDSL depend some extent upon impulsive noise immunity, those numbers can be reasonably reduced for DMT in HDSL.

Of course, the price paid for the added immunity is the latency, which at 1–3 ms is still well within acceptable limits for latency in the loop transceiver system itself.

### *B. Discussion*

A computer simulation of the specific transmitter and receiver in Figs. 4 and 6, respectively, was used to process several hundred million samples of randomly generated transmit data over an HDSL channel with the characteristics of loop *H*. The total loss in performance that accrues to the various approximations and assumptions made throughout our analysis was found to be less than a 0.2 dB increase in noise power. An actual real-time implementation of the DMT HDSL transmission system has been constructed by the authors, but measured results from it were not available at the time of this writing.

Our results clearly illustrate fundamental tradeoffs between performance and computational requirement. For instance, larger blocklengths and higher sampling rates can always lead to performance improvement. Also, increasing transmit power can always improve performance. Nevertheless, our results indicate that a system with blocklength $N + \nu = 520$ and an $L = 10$ tap feedforward equalizer at sampling rate 640 kHz with 10 mW of transmit power is sufficient to achieve the desired data rates at the target error rate of $10^{-7}$ on nearly all CSA channels. Our projected computational requirement on a representative DSP (Motorola 56000) indicate that these numbers lead to a DMT transceiver that is practical for

then two IFFT's, two

implementation. Further, both the transmitter (near end) and receiver (far end) could be implemented on a single programmable DSP (with considerable compute power remaining for echo cancellation) if that DSP were custom designed so that it had an FFT peripheral in addition to the standard multiply-accumulate arithmetic unit. This estimate, however, does not include the implementation of the Viterbi decoder for any applied trellis code. Nevertheless, a programmable Viterbi signal processor has been proposed [33] that could, on a single VLSI circuit, implement any of the codes that were used in this study.

Theoretically, it has been shown [20], [34] that decision feedback systems can be designed to achieve almost as high performance as DMT systems if the DFE system is allowed infinite complexity. Such systems require knowledge of the channel at the transmitter (as does DMT) in the form of both a Tomlinson precoder, an optimized transmit filter, and an optimized sampling rate. The code used in the DFE system is the same in performance and complexity as the one used in the DMT system. A detailed study in [9] showed that approximately 128 total tap coefficients, feedforward and feedback combined, were needed by a decision feedback equalizer that was optimized and performed close to the same as the specific DMT system analyzed in this paper. An adaptive equalizer with 128 taps required in excess of 100 MIPS of processing power, which is significantly more than the DMT system's 30 MIPS.

There are other practical advantages of DMT with respect to baseband systems (like 2B1Q). One is improved tolerance to impulse noise and the ability to shape the transmit spectrum automatically. For instance, some of the subchannels in the lower 4 kHz will reliably transmit data even on a disfunctioning HDSL channel, such as one that has not had a loading coil removed, thus allowing routine maintenance functions on a channel that would otherwise be useless with baseband transmission. Another advantage is the possibility of a cost-effective programmed transmitter and receiver combination that would permit modification or alteration of function through software change (rather than redesign of a custom VLSI circuit) should unforseen problems arise during field testing. A third advantage is the cost reduction that occurs when using the service in the single-duplex mode. The transmitter that is used for dual-duplex is already cost effective but also sufficiently powerful to transmit 1.6 Mb/s on a single twisted pair reliably, albeit with reduced margin. This is because the second line interface and analog-to-digital interfaces need not be duplicated, and also because no (other) hardware changes are necessary (only software) to implement the single duplex. The possibility of the single-duplex service being far more desirable than the dual-duplex has already been espoused by some potential HDSL customers [35], as sufficient copper for the two-twisted-pair service may not exist in many areas. A fourth practical advantage is that services such as the asymetric digital subscriber line (ADSL) can also be implemented via software change in the implementing hardware [36].

## V. Conclusion

We conclude that, by using a discrete multitone modulation technology, almost all CSA loops can sustain reliable transmission of 1.6 Mb/s on a single wire pair with 6 dB margin. With two twisted pairs, the cost increases because of the extra interface circuitry, but so does the margin or tolerance to unforseen line difficulties.

We further conclude that the DMT system, while nearly having the highest performance that is practically achievable, simultaneously has the lowest computational requirement. This low cost can be translated into a software-controlled cost-effective HDSL transceiver product. It is for these reasons, and other more detailed reasons described within, that we conclude that a DMT transceiver system is the best possible technical alternative for the HDSL application.

## Appendix
## Effect of Cyclic Prefix on Average Input Energy

Let the input to the IFFT be denoted by $u_k$ and $v_k$ for the independent real and imaginary part, respectively. With a blocklength of $N$, the block of data symbol going to the inverse FFT is denoted by $\vec{G}$:

$$\vec{G} = [u_0 + jv_0 \quad u_1 + jv_1 \quad u_2 + jv_2 \cdots u_{N/2} + jv_{N/2} \cdots u_{N-1} + jv_{N-1}]. \tag{23}$$

Since the input data to the channel needs to be real, Hermitian symmetry is required:

$$v_0 = v_{(N/2)} = 0 \tag{24}$$

$$u_i = u_{N-i}, \qquad v_i = -v_{N-i}, \qquad i = 1, 2, \cdots, \frac{N}{2} - 1. \tag{25}$$

$E[u_k]$ and $E[v_k]$ are zero, and for $k, l \leq N/2$:

$$E[u_k u_l] = E[v_k v_l] = 0, \qquad k \neq l \tag{26}$$

$$E[u_k v_l] = 0. \tag{27}$$

We also denote the average energy as:

$$E[u_k^2] = \sigma_{u_k}^2 \qquad E[v_k^2] = \sigma_{v_k}^2. \tag{28}$$

The output of the inverse FFT, $\vec{X}$, is then:

$$\vec{X} = \text{IFFT}\{\vec{G}\} = [X_0 \quad X_1 \cdots X_{N-1}] \tag{29}$$

where

$$X_m = \frac{1}{\sqrt{N}} \sum_{k=0}^{N-1} (u_k + jv_k) e^{j(2\pi km/N)}. \tag{30}$$

Applying (24) and (25) and simplifying, we obtain:

$$X_m = \frac{1}{\sqrt{N}} \left[ u_0 + u_{(N/2)} e^{j\pi m} + 2 \sum_{i=1}^{(N/2)-1} \left( u_i \cos \frac{2\pi im}{N} - v_i \sin \frac{2\pi im}{N} \right) \right] \tag{31}$$

so $E[X_m] = 0$ from (26) and (27). And

$$E[X_m^2] = \frac{1}{N}\left\{\sigma_{u0}^2 + \sigma_{u(N/2)}^2 + 4\sum_{i=1}^{(N/2)-1}\left[\sigma_{u_i}^2 \cos^2\left(\frac{2\pi im}{N}\right) + \sigma_{v_i}^2 \sin^2\left(\frac{2\pi im}{N}\right)\right]\right\}. \quad (32)$$

Define

$$\epsilon_x \triangleq \frac{1}{N}\sum_{i=0}^{N-1} E[X_i^2] = \frac{1}{N}\left[\sigma_{u0}^2 + \sigma_{u(N/2)}^2 + 2\sum_{i=1}^{(N/2)-1}(\sigma_{u_i}^2 + \sigma_{v_i}^2)\right]. \quad (33)$$

For general case, that is, if $\sigma_{u_k}^2 \neq \sigma_{v_k}^2$ for some $k$, then the sum of the energy of any $\nu$ consecutive samples of $\vec{X}$ is:

$$\sum_{i=M}^{M+\nu-1} E[X_i^2] = \frac{1}{N}\left\{\nu(\sigma_{u0}^2 + \sigma_{u(N/2)}^2) + 4\sum_{l=1}^{(N/2)-1}\left[\sigma_{u_l}^2 \sum_{n=M}^{M+\nu-1}\cos^2\left(\frac{2\pi ln}{N}\right) + \sigma_{v_l}^2 \sum_{n=M}^{M+\nu-1}\sin^2\left(\frac{2\pi ln}{N}\right)\right]\right\} \quad (34)$$

where $M$ is the starting point of the $\nu$ samples.

There is no closed form expression for arbitrary values of $\nu$ and $M$. However, for sufficiently large $N$ (such as 64 and above) and $\nu \geq 2$, then

$$\sum_{i=M}^{M+\nu-1} E[X_i^2] \approx \frac{1}{N}\left\{\nu(\sigma_{u0}^2 + \sigma_{u(N/2)}^2) + 2\nu\sum_{l=1}^{(N/2)-1}[\sigma_{u_l}^2 + \sigma_{v_l}^2]\right\} = \nu\epsilon_x \quad (35)$$

so the average energy of a block of $N + \nu$ samples $\vec{X}_{CE}$ (after cyclic extension by $\nu$ samples) is given by:

$$E[\vec{X}_{CE}\vec{X}_{CE}^T] \approx (N + \nu)\epsilon_x \quad (36)$$

where $\vec{X}_{CE}$ is a row vector.

To ensure the average energy of the block $\vec{X}_{CE}$ is strictly less than a given energy constraint, we can define $\sigma_{t_k}^2$ as the larger of $\sigma_{u_k}^2$, $\sigma_{v_k}^2$:

$$\sigma_{t_k}^2 = \max\{\sigma_{u_k}^2, \sigma_{v_k}^2\} \quad (37)$$

then

$$E[X_m^2] \leq \frac{1}{N}\left[\sigma_{t0}^2 + \sigma_{t_{(N/2)}}^2 + 4\sum_{i=1}^{(N/2)-1}\sigma_{t_i}^2\right] \triangleq \epsilon_t \quad (38)$$

and

$$E[\vec{X}_{CE}\vec{X}_{CE}^T] \leq N\epsilon_x + \nu\epsilon_t \quad (39)$$

a simple and fairly tight bound for sufficiently large $N$.

In the case of equal energy among the real and imaginary part, $\sigma_{u_k}^2 = \sigma_{v_k}^2$:

$$E[X_m^2] = \frac{1}{N}\left[\sigma_{u0}^2 + \sigma_{u(N/2)}^2 + 4\sum_{i=1}^{(N/2)-1}\sigma_{u_i}^2\right] = \epsilon_x \quad (40)$$

*independent* of $m$. This means that each sample at the output of the IFFT has the same average energy $\epsilon_x$, and

$$E[\vec{X}_{CE}\vec{X}_{CE}^T] = (N + \nu)\epsilon_x \quad (41)$$

which means that the cyclic prefix does not change the energy constraint.

## Acknowledgment

The authors would like to thank the following people, in alphabetical order, for helpful discussions and suggestions throughout the development of this paper: N. Jablon of AT&T, P. Crespo, R. Hsing, and J. Lechleider of Bell Communication Research, P. Algoet, J. Aslanis, P. Chow, G. Dudevoir, M. Ho, S. Kasturia, H. Lou, A. Ruiz, and R. Ziegler of Stanford University, and J. Bingham of Telebit.

## References

[1] M. L. Doelz, E. T. Heald, and D. L. Martin, "Binary data transmission techniques for linear systems," *Proc. IRE*, vol. 44, pp. 656–661, May 1957.
[2] I. Kalet, "The multitone channel," *IEEE Trans. Commun.*, vol. 37, no. 2, pp. 119–124, Feb. 1989.
[3] A. Ruiz, J. M. Cioffi, and S. Kasturia, "Discrete multiple tone modulation with coset coding for the spectrally shaped channel," to appear in *IEEE Trans. Commun.*
[4] J. A. C. Bingham, "Multicarrier modulation for data transmission: An idea whose time has come," *IEEE Commun. Mag.*, vol. 28, no. 5, pp. 5–14, May 1990.
[5] B. Hirosaki, S. Hasegawa, and A. Sabato, "Advanced groupband data modem using orthogonally multiplexed QAM technique," *IEEE Trans. Commun.*, vol. 34, no. 6, pp. 587–592, June 1986.
[6] J. T. Aslanis and J. M. Cioffi, "Achievable information rates on digital subscriber loops: Limiting information rates with crosstalk noise," to appear in *IEEE Trans. Commun.*
[7] J. S. Chow, J. C. Tu, and J. M. Cioffi, "A computationally efficient adaptive transceiver for high-speed digital subscriber lines," presented at the 1990 Int. Conf. Commun., Atlanta, GA, Apr. 1990.
[8] J. C. Tu and J. M. Cioffi, "A loading algorithm for the concatenation of coset codes with multichannel modulation methods," presented at the 1990 Global Commun. Conf., San Diego, CA, Dec. 1990.
[9] G. P. Dudevoir, J. S. Chow, S. Kasturia, and J. M. Cioffi, "Combined equalization and coding for T1 data rates on carrier serving area subcriber loops," presented at the 1989 Int. Conf. Commun., Boston, MA, June 1989.
[10] J. W. Lechleider, "High bit rate digital subscriber lines: A review of HDSL progress," this issue, pp. 769–784.
[11] Bell Communications Research, "High bit-rate digital subscriber line (HDSL) systems that support DS1 rate access in the copper loop plant," Bellcore Req. Inform., RFI 90-03, Mar. 1990.
[12] P. M. Crespo, Bell Commun. Res., private communication, Aug. 1988.
[13] T. Starr and M. Day, Ameritech, private communication, Sept. 1989.
[14] J. A. C. Bingham, private communication, Oct. 1990.
[15] D. G. Messerschmitt, "Design issues in the ISDN U-interface transceiver," *IEEE J. Select. Areas Commun.*, vol. 4, pp. 1281–1293, 1986.
[16] S. Cox and P. Adams, "An analysis of digital transmission techniques for the local network," *British Telecom Tech. J.*, vol. 33, July 1985.

subch... then two IFFT's, two ...

[17] D. W. Lin, "Wide-band digital subscriber access with multidimensional block modulation and decision feedback equalization," *IEEE J. Select. Areas Commun.*, vol. 7, no. 6, pp. 996-1005, Aug. 1989.
[18] E. Arnon, "Impulse noise immunity of HDSL systems," ANSI contrib. T1E1.4/90-170, Sept. 24, 1990.
[19] G. D. Forney Jr., "Coset codes I: Introduction and geometrical classification," *IEEE Trans. Inform. Theory*, vol. 34, no. 5, pp. 1123-1151, Sept. 1988.
[20] J. M. Cioffi, G. P. Dudevoir, M. V. Eyuboglu, and G. D. Forney Jr., "MMSE decision-feedback equalizers and coding—Part I: General results," submitted for publication to *IEEE Trans. Commun.*
[21] G. J. Pottie and M. V. Eyuboglu, "Combined coding and precoding for PAM and QAM HDSL systems," this issue, pp. 861-870.
[22] N. Zervos, "Transmission near capacity over the local cable network using the carrierless AM/PM couple sideband modulation—Part I: The uncoded case," *IEEE J. Select. Areas Commun.*
[23] J. M. Cioffi, "Least-squares storage channel identification," *IBM J. Res. Devel.*, vol. 30, no. 3, pp. 310-320, May 1986.
[24] S. M. Kay, *Modern Spectral Estimation: Theory and Applications.* Englewood Cliffs, NJ: Prentice-Hall, 1988.
[25] L. Ljung, *System Identification: Theory for the User.* Englewood Cliffs, NJ: Prentice-Hall, 1987.
[26] J. A. C. Bingham and J. M. Cioffi, "A data-driven multitone echo canceller," submitted for publication to *IEEE Trans. Commun.*
[27] G. Davidson and D. Falconer, "Reduced complexity echo cancellation using orthonormal functions," *IEEE Trans. Circ. Syst.*, vol. 38, no. 1, pp. 20-28, Jan. 1991.
[28] M. Ho, J. Tu, and J. M. Cioffi, "A parametric estimator for reduced complexity echo cancellation," presented at the 1991 IEEE HDSL Workshop, Sunnyvale, CA, June 1991.
[29] G. D. Forney Jr., R. G. Gallager, G. R. Lang, F. M. Longstaff, and S. U. Qureshi, "Efficient modulation for band-limited channels," *IEEE J. Select. Areas Commun.*, vol. SAC-2, no. 5, Sept. 1984.
[30] K. Kerpez, "Near end crosstalk is almost Gaussian," submitted for publication to *IEEE Trans. Commun.*
[31] L. F. Wei, "Trellis-coded modulation with multidimensional constellations," *IEEE Trans. Inform. Theory*, vol. 33, no. 4, pp. 483-501, July 1987.
[32] G. D. Forney Jr., "Trellis constellations," submitted for publication to *IEEE Trans. Inform. Theory.*
[33] H. Lou and J. M. Cioffi, "A programmable parallel processor architecture for Viterbi detection," presented at the 1990 Global Commun. Conf., San Diego, CA, Dec. 1990.
[34] N. Zervos and I. Kalet, "Optimized decision feedback equalization versus optimized orthogonal frequency division multiplexing for high-speed data transmission over the local cable network," presented at the 1989 Int. Conf. Commun., Boston, MA, June 1989.
[35] A. Ghanem, Southwest Bell Corp., private communication, Nov. 1990.
[36] P. S. Chow, J. C. Tu, and J. M. Cioffi, "Performance evaluation of a multichannel transceiver system for ADSL and VHDSL services," this issue, pp. 909-919.

**Jacky S. Chow** (S'86) was born in Hong Kong in 1966. He received the B.S. degree in electrical engineering (summa cum laude) from the California State University, Fresno, in 1987, and the M.S. degree in electrical engineering from Stanford University, Stanford, CA, in 1988.

He is currently pursuing the Ph.D. degree in electrical engineering at Stanford University. His current research interests include digital communications, coding, digital signal processing, computer networks, algorithms, and complexity involved in real-time implementation of digital communication systems.

**Jerry Tu** (S'86) was born in Rio de Janeiro, Brazil, in 1961. He received the B.S. degree in general engineering from Harvey Mudd College, Claremont, CA, in 1982, the S.M. degree in electrical engineering from the Massachusetts Institute of Technology, Cambridge, in 1984, and the Ph.D. degree in electrical engineering from Stanford University, Stanford, CA in 1991.

From 1984 to 1986, he was a Member of Technical Staff with Hughes Aircraft Company, Fullerton, CA, where he developed spread spectrum tactical communication systems, specializing in acquisition, synchronization, and tracking of direct sequenced signals. At Stanford University, his research interests were in the field of communication theory, coding, equalization, and real-time implementation of digital communication systems. He is currently with a private company developing high-speed digital communication modems for data, voice, and video applications on the telephone channel.

**John M. Cioffi** (S'77-M'78-SM'90) for a photograph and biography, see p. 764.